



# Design and development of an electroanalytical sensor based on molecularly imprinted polyaniline for the detection of thyroxine

Deepanmol Singh<sup>1</sup> · Souradeep Roy<sup>1,2</sup> · Neeraj Mahindroo<sup>3</sup> · Ashish Mathur<sup>2</sup>

Received: 13 April 2023 / Accepted: 8 July 2023 / Published online: 20 July 2023  
© The Author(s), under exclusive licence to Springer Nature B.V. 2023

## Abstract

Hypothyroidism and hyperthyroidism are one of the most frequently observed endocrine disorders in the world. Failure to undergo timely diagnosis and treatment often results in life-threatening events such as arrhythmia, hypertension, and cardiac arrest to name a few. Considering the various limitations of conventional diagnostic strategies, early, accurate, and efficient diagnoses of these disorders are pivotal for their timely management. In the present work, a molecularly imprinted polymer (MIP)-based sensor is developed for the detection of thyroxine ( $T_4$ )—the key biomarker. This has been achieved by templating  $T_4$  into polyaniline matrix supported on indium tin oxide-coated glass electrodes. The chemical synthesis of polyaniline was done through oxidative polymerization and optimized using response surface methodology. The optimum condition for ultrasonication-based extraction of  $T_4$  from polyaniline matrix was 15 min at 30 °C with 75 mM NaOH. The imprinting factor was found to be 1.98. The developed MIP-based sensor was characterized using chromatographic, spectroscopic, and electrochemical techniques. The sensor calibration was obtained within  $T_4$  concentration range of 5–50  $\text{pg mL}^{-1}$ , with a calculated limit of detection of 6.16  $\text{pg mL}^{-1}$ . Repeatability studies show a relative standard deviation of 2.45%. Recovery from saliva was found to be between 96 and 115.2%. The developed MIP-based electroanalytical sensor was found to exhibit a high degree of selectivity against various interferants and thereby possessing huge prospects toward futuristic point-of-care applications.

---

✉ Deepanmol Singh  
deepanmol.niper@gmail.com

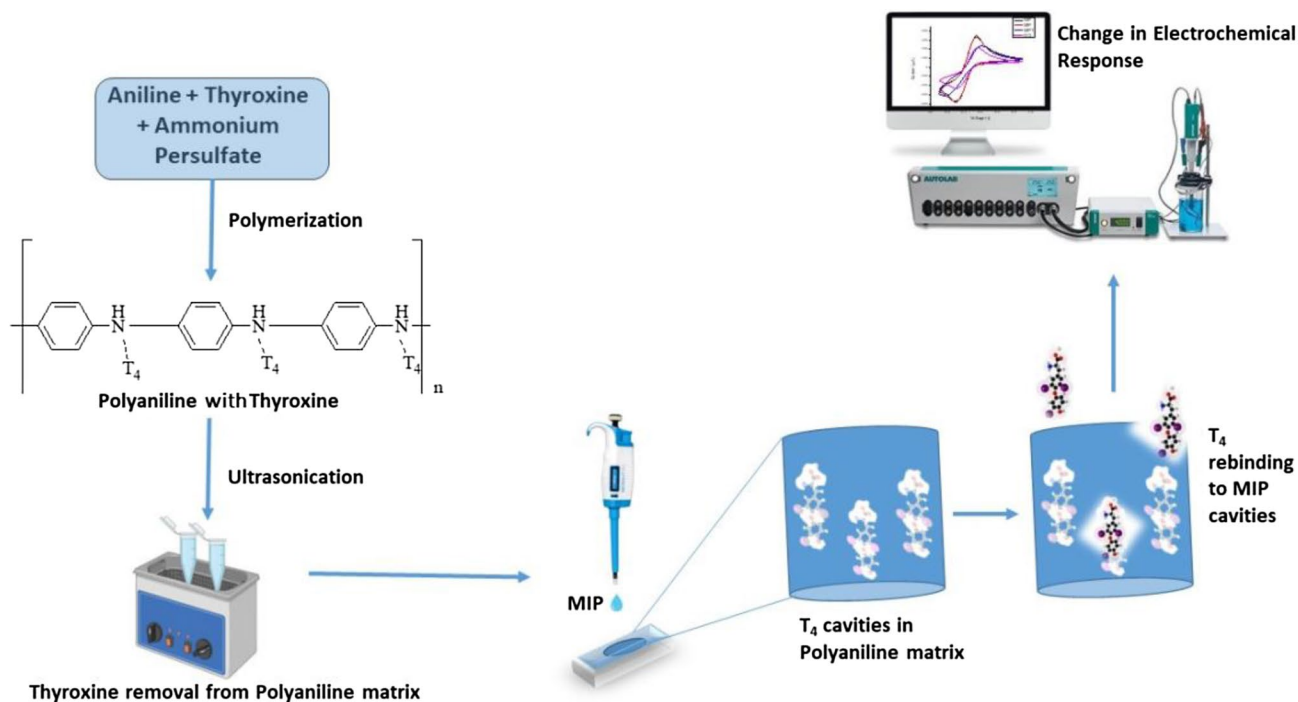
Ashish Mathur  
nanoashish@gmail.com

<sup>1</sup> School of Health Sciences and Technology, University of Petroleum and Energy Studies (UPES), Dehradun, India

<sup>2</sup> Centre for Interdisciplinary Research and Innovation (CIDRI), University of Petroleum and Energy Studies (UPES), Dehradun, India

<sup>3</sup> School of Pharmacy, Dr. Vishwanath Karad MIT World Peace University, Pune, Maharashtra, India

## Graphical abstract



**Keywords** Thyroid disorders · Thyroxine (T<sub>4</sub>) · Biosensor · Molecularly imprinted polyaniline · Electrochemical transduction · Point-of-care

## 1 Introduction

Due to increasing sedentary lifestyle, majority of people around the world underestimate the biological changes happening in the body. These changes are often related to hormonal imbalance which further translates into life-threatening events. There are reports of sudden deaths in young population globally which could be correlated to minor fluctuations in the levels of hormones. These changes lead to serious metabolic events in the body, which can eventually result in chronic ailments. One of the major contributors of hormonal fluctuations in human body is thyroid gland which produces metabolic hormones such as thyroxine and liothyronine [1, 2]. Among these, thyroxine (T<sub>4</sub>) is highly crucial which is secreted into the bloodstream from the thyroid gland, which influences metabolism, oxygen synthesis, and protein synthesis [3]. The concentration of T<sub>4</sub> in serum generally varies within 8–18 pg mL<sup>-1</sup> [4], and any abnormal deviation leads to a multitude of life-threatening events such as hypertension, arrhythmia, and acute myocardial infarction to name a few. Furthermore, the regulation of T<sub>4</sub> is strongly associated with cognitive health, since undesired fluctuations result in depression which is eventually leads to deterioration

of physical well-being [5, 6]. Therefore, timely detection of T<sub>4</sub> in bodily fluids is the need-of-hour in order to avert serious health complications and associated comorbidities.

The current diagnostic methods for the identification of T<sub>4</sub> include chromatography [7], mass spectroscopy [8], and immunological analysis [9]. However, these techniques are time consuming, costly, and require bulky benchtop equipment and skilled manpower for their operation. Such impediments often result in delayed diagnosis and treatment and can lead to debilitating outcomes. Therefore, there is a requirement for the development of next-generation diagnostic platforms for early and efficient detection of thyroid disorder, as a function of T<sub>4</sub> concentrations.

In recent years, there has been increasing interest in electrochemical biosensing techniques as they are cost-effective, efficient, provide rapid response, and easy to translate toward connected health applications [10, 11]. Out of the commonly employed various electroanalytical techniques (enzymatic, immunosensing, genosensing, MIPs), MIP-based techniques overweigh others due to their high selectivity, long-term stability, and chemical inertness [12]. Several studies have shown the applicability of molecularly imprinted polymers for electrochemical estimation of biological compounds including dopamine, phenylalanine, etc. [13–15].

MIPs are known as synthetic receptors and they have shown usefulness in the field of environmental remediation, biotechnological processes, extraction process, and as sensing materials [6, 12, 16–18].

From the biosensing viewpoint, molecular imprinting results in the formation of analyte-specific binding sites which are highly stable and resistant to harsh temperatures as well as acidic/basic conditions [19]. MIP-based techniques have been successful in selective quantification of specific compounds present in biological matrices. The high degree of selectivity and sensitivity of MIP technology has been used by several researchers for quantification of biomarkers for diabetes, hypertension, infectious diseases, etc. [20–23]. However, the application of MIPs for  $T_4$  detection is least explored. Polyaniline (PANI) is one of the most commonly used conducting polymer due to its conductive properties, fast response and better sensitivity. It has been previously used for the determination of several biological molecules of human body [24].

We endeavored the fabrication of imprinted polyaniline film on indium tin oxide (ITO) electrode for the electrochemical determination of thyroxine. This study will enhance the development of point-of-care diagnosis of thyroxine and hence would increase the patient compliance.

## 2 Materials and methods

### 2.1 Materials and reagents

Thyroxine (levothyroxine) was procured from Macleods Pharmaceuticals Limited, India. Liothyronine was purchased from Merck (Darmstadt, Germany). Aniline and ammonium persulfate were purchased from Rankem and Loba Chemie Pvt. Ltd. respectively. High-performance liquid chromatography (HPLC) grade methanol was procured from Rankem (India). Phosphate buffer solution (PBS, pH 3) was prepared with potassium dihydrogen phosphate ( $KH_2PO_4$ ) and

phosphoric acid both from Rankem. Ultrapure water (resistivity  $\sim 18.2 \Omega \text{ cm}$  at 298 K) from water purification system (Milli-Q system Millipore Bedford, MA, USA) was used in all HPLC experiments. ITO-coated glass electrodes (Thickness—1.1 mm, Resistivity  $\leq 10 \text{ ohms sq}^{-1}$ ) were purchased from Tech instro Industries, India. All the chemicals procured were of highest analytical grade and did not require further purification. Freshly prepared working solutions for electrochemical sensing were used.

### 2.2 Synthesis of MIPs

Polyaniline was synthesized chemically using aniline as monomer and ammonium persulfate as redox initiator. The reaction was performed in an acidic environment by initially preparing two aliquots. Solution A: 1.8 g of ammonium persulfate was added in 45 mL of 0.1 N HCl. Solution B: 0.25 mL of aniline and 5 mg of thyroxine was added in 150 mL of 0.1 N HCl and the mixture was thoroughly stirred using magnetic stirrer at 300 rpm for 30 min. Solution A was added to solution B dropwise and the final mixture was kept for 1 h before the product was separated through filtration. The filtered product was finally air dried at ambient temperature [25].

The same procedure was repeated without the addition of thyroxine in solution B to synthesize non-imprinted polymer (NIP) as shown in Fig. 1.

The blue-colored solid product of polyaniline without thyroxine (NIP) and with thyroxine (MIP+ $T_4$ ) was formed. In the next step, geometry-specific cavities were generated by removing thyroxine from the polyaniline matrix. This was achieved by ultrasonating 20 mg of  $T_4$ -polyaniline hybrids in 2 mL of 0.075 M NaOH for 15 min at 30 °C. The step was repeated three times to ensure the significant removal of thyroxine. These conditions were optimized for the critical variables including time, temperature, and concentration of NaOH, as discussed in Sect. 2.3. After sonication,

**Fig. 1** Synthesis reactions of non-imprinted (without  $T_4$ ) and molecularly imprinted polyaniline (with  $T_4$  addition)

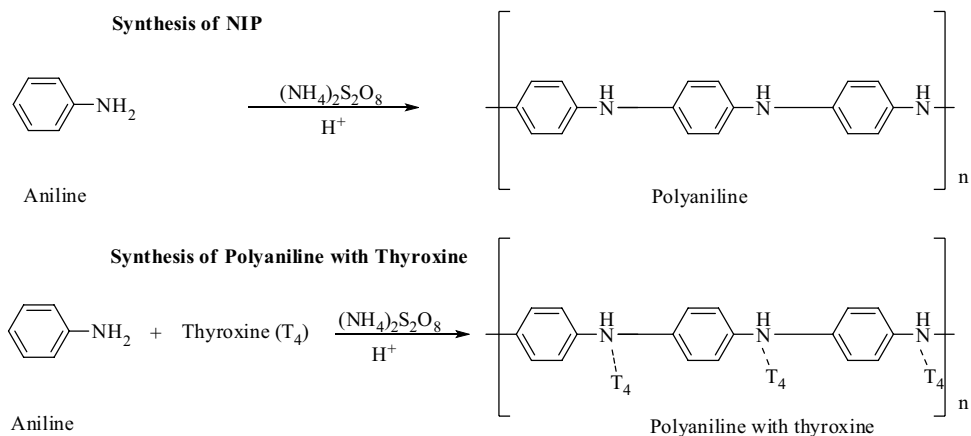


**Table 1** Parameters for HPLC analysis for studying thyroxine removal from the matrix [26]

Conditions	Parameters
Column	Reverse phase C-18 column, 4.6×250 mm and 5 μm particle size
Mobile phase	Methanol—solvent A Phosphate buffer pH 3—solvent B
Gradient	45–20% Solvent A in 7 min 20% Solvent A for 7–12 min 20–45% Solvent A for 12–16 min 45% Solvent A for 16–20 min
Injection volume	20 μL
Flow rate	1 mL min <sup>-1</sup>
Wavelength	228 nm

**Table 2** Different factors and levels selected for optimization study

Factors	Lower level	Intermediate level	Upper level
Temperature	30 °C	40 °C	50 °C
Concentration of NaOH	75 mM	100 mM	125 mM
Time of sonication	15 min	30 min	45 min

the product was air dried and was used for characterization studies and electrochemical analysis.

### 2.3 Optimization of template removal

HPLC method was employed to study the thyroxine removal from polyaniline matrix. The optimized method for HPLC analysis is given in Table 1.

The chromatographic analysis using HPLC was performed for pure thyroxine, supernatant of polyaniline containing thyroxine obtained by sonication (for different conditions shown in Table 2), and for supernatant of NIP. Samples without sonication step were used as negative control. The process is explained in Fig. 2.

Optimization studies for thyroxine removal were performed by varying three parameters, namely, temperature,

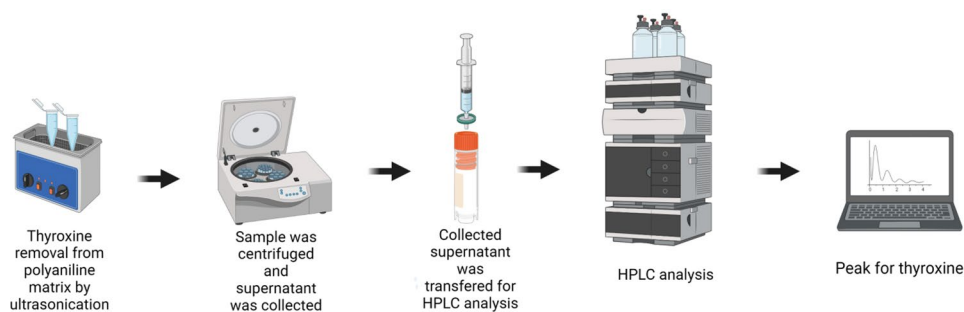
concentration of NaOH, and sonication time. Response surface design (Box Behnken Design) was used to study the removal of thyroxine from the polyaniline matrix. The design was prepared and analyzed using Design Expert 13 software (Stat ease, Minneapolis, USA). The area under the peak from chromatogram was considered as the response parameter for the trial, with the factors and levels being summarized in Table 3. In all, fourteen different combinations were evaluated based on selected conditions derived from Design Expert 13 software.

Imprinting factor was calculated by incubating thyroxine (10 μg mL<sup>-1</sup>) with MIP (20 mg) and NIP (20 mg) for 3 h under constant stirring. The mixtures were then centrifuged at 10,000 rpm for 10 min at 10 °C and the supernatant was analyzed with HPLC. The same HPLC conditions were used as mentioned in the previous section. The peaks areas were used to determine the concentration of free thyroxine in supernatant.

### 2.4 Characterization studies of MIPs and NIPs

The micro-structural characterization of NIP and MIP surfaces was performed using techniques such as Fourier transform infrared spectroscopy (FT-IR), atomic force microscopy (AFM), and contact angle measurements. The latter was also used to calculate the surface energy of NIP and MIP coated electrodes.

FT-IR analysis was performed for NIP, MIP, and T<sub>4</sub>-MIP solutions. Approximately 2 mg of sample was mixed with potassium bromide and a pellet was formed. The sample was then analyzed in 400–4400 cm<sup>-1</sup> range. AFM scan was performed on 10×10 μm surface. The scans were performed for both non -imprinted and imprinted polyaniline coated onto a glass slide by drop cast method. Contact angle analysis was performed by drop shape analyser (DSA25Kruess, Germany). To calculate the surface energy, a drop of milliQ water (polar solvent) and ethylene glycol (non-polar solvent) were dropped separately onto a slide coated with MIP and NIP. The study was repeated three times.

**Fig. 2** Schematic diagram for the optimization of T<sub>4</sub> removal process from polyaniline-T<sub>4</sub> composite

## 2.5 Electrochemical analysis

Electrochemical analysis was performed using a Metrohm Dropsens electrochemical potentiostat (uStat i-400) using the three-electrode setup. In this case, MIP-coated ITO acting as the working electrode while Ag/AgCl and Pt served as reference and counter electrodes, respectively. Cyclic voltammetry (CV) electrochemical impedance spectroscopy (EIS) experiments were performed for electrochemical study. All electrochemical studies were performed in potassium ferro-ferricyanide solution (10 mM) prepared in phosphate buffer saline (1 mM, pH 7.4).

## 2.6 Sensor fabrication

The synthesized molecularly imprinted polyaniline was introduced onto ITO-coated glass electrode by drop-drying method (Fig. 3). Electrodes with 10 mm × 7 × 1.1 mm dimensions were used for the study. Molecularly imprinted polyaniline (5 μL) was drop casted onto the ITO electrode and was kept in an oven at 60 °C for 45 min. The electrodes were then rinsed with water and air dried before using for electrochemical study.

These coated electrodes were used for electrochemical characterization studies using CV and electrochemical impedance spectroscopy (EIS), scan rate study, incubation studies, linearity studies, repeatability, interference studies, and recovery from saliva sample.

For EIS, the frequency scan was performed from 10 kHz to 1 MHz. Randel's circuit simulation of impedance spectra was done using Zview software.

Scan rate study was done in a potential range of –0.1–0.9 V starting from 10 mV s<sup>-1</sup> till 180 mV s<sup>-1</sup>. Incubation study was performed using 10 μL of 20 ng mL<sup>-1</sup> of thyroxine onto MIP sensor and the CV response was observed between –0.1 and 0.9 V potential at a scan rate of 50 mV s<sup>-1</sup>. Different time intervals for incubation

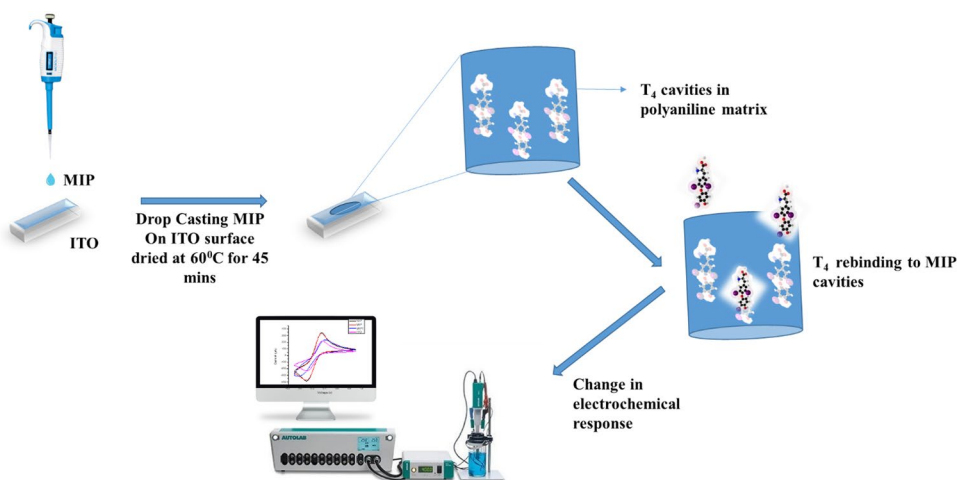
study were 2 min, 4 min, 6 min, 8 min, 10 min, 12 min, and 14 min.

Linearity studies were performed using freshly prepared solutions of concentrations 5 to 50 pg mL<sup>-1</sup>. Several MIP-coated ITO electrodes were prepared and incubated with different concentrations of thyroxine. The sample (5 μL) was added onto the coated ITO and incubation was done at RT for 10 min. Repeatability studies were performed at 50 pg mL<sup>-1</sup> using 5 independent coated ITO electrodes. All the electrodes were washed with distilled water to remove any surface-bound thyroxine before electrochemical analysis.

Interference studies were performed using biomolecules structurally similar to thyroxine. The molecules selected for the study were phenylalanine, tyrosine, and liothyronine. The concentration of these molecules for interference studies was taken as 100 × 10<sup>6</sup> pg mL<sup>-1</sup> for tyrosine and phenylalanine and 5 × 10<sup>3</sup> pg mL<sup>-1</sup> for liothyronine. Concentration of the tyrosine and phenylalanine was selected so as to simulate the biological conditions but the concentration of free liothyronine is taken more than that present in the body. Liothyronine levels are naturally 100 times less than T<sub>4</sub>, and at such low levels, it won't practically interfere with thyroxine. However, the selected liothyronine concentration would be relevant for studying interference if the proposed method is to be used for the assay of pharmaceutical tablets thyroxine. Liothyronine can be present in thyroxine tablets (dose range 5 to 100 μg) as an adulterant or a degradation product [27].

Human saliva was taken by directly spitting into a test tube. Before sample collection, the mouth was thoroughly rinsed with water (15 min prior to sample collection). The obtained samples were diluted with 5 mL of water. The samples were then filtered using 0.22-μm syringe filter and stored at 4 °C. Real sample analysis was performed by spiking the saliva samples with 50 pg mL<sup>-1</sup>.

**Fig. 3** Representation of different steps of electrode fabrication and electrochemical sensing



### 3 Results and discussion

#### 3.1 Molecularly imprinted solid-phase extraction (MI-SPE) analysis

HPLC chromatograms showed differences at each stage of MIP synthesis (Fig. 4). HPLC chromatogram (Fig. 4a) of pure thyroxine showed a sharp peak around 10 min of scan time. This signature peak of thyroxine was used as a

positive control. Polyaniline with thyroxine after sonication at 30 °C for 15 min with 75 mM NaOH solution also showed a peak at 10 min. This confirms that thyroxine was extracted by sonication (Fig. 4b). To further support the results, NIP was also sonicated with similar conditions and no peak was observed around 10 min (Fig. 4c). A negative control (without sonication) showed a very small peak at 10 min in HPLC chromatogram (Fig. 4d). This small peak shows the removal of some weakly adsorbed surface adsorbed thyroxine on polyaniline matrix. As HPLC

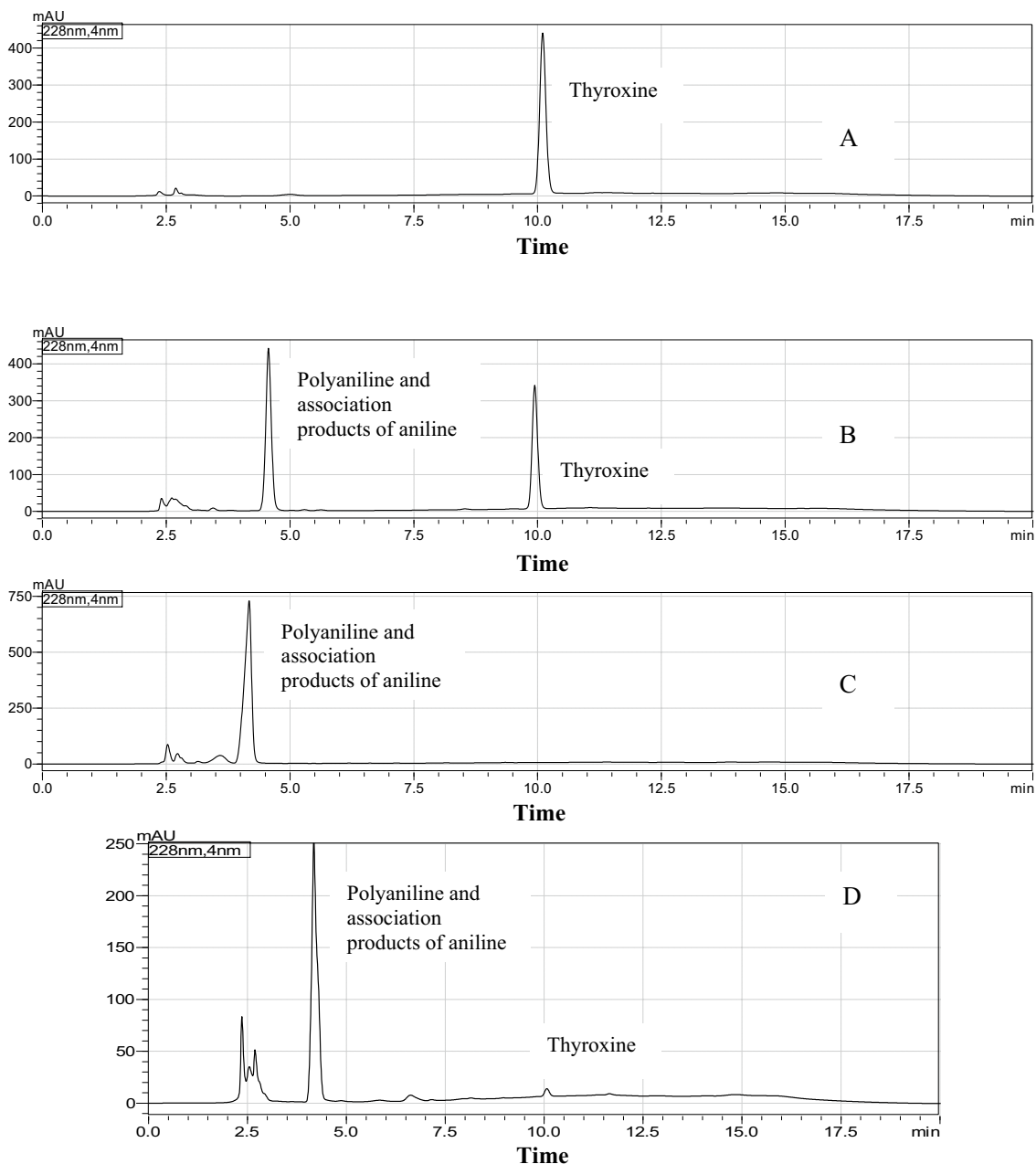


**Fig. 4** a Chromatogram of pure thyroxine b chromatogram after extraction from NIP c chromatogram after extracted from polyaniline with T<sub>4</sub> d chromatogram after three consecutive extractions from polyaniline



peak area is proportional to the concentration of analyte, hence, the negative control results highlight the importance of sonication process, as without sonication, very small amount of thyroxine was removed [28].

The extraction results of thyroxine from polyaniline matrix with different conditions using design of experiment (DoE) approach are shown in Table 3. The maximum peak area in Run 13 gives the best conditions for thyroxine removal.

A linear model was found to be significant with model equation.

$$\text{Sqrt}(R1) = + 20012.80449 - 161.11872 \text{ mol} - 392.35263 \text{ temp} + 3.38411 \text{ mol} * \text{temp}. \quad (1)$$

The model formed was found to be significant with *f* value of 4.93. *P* values were less than 0.05. Adequate precision was found to be 7.348 (greater than 4 is desirable). A value of 7.348 indicates an adequate signal [29]. According to the Eq. (1), time did not had a significant effect in the removal of T<sub>4</sub>.

The best response obtained was with lowest concentration, low temperature, and less time; hence, 75 mM NaOH, 30 °C, and 15 min were selected as extraction conditions. Using these conditions, sonication was performed multiple times until no trace of thyroxine was observed in HPLC. The 3D plot (Fig. 5) shows the change in response with change in temperature and molarity for fixed time 30 min.

To evaluate the specific binding property of MIP and NIP toward thyroxine and to highlight the non-specific interactions that result from the thyroxine adsorption, the imprinting factor (IF) has been calculated using Eq. (2):

$$IF = \frac{B(\text{MIS}) \times F(\text{NIS})}{F(\text{MIS}) \times B(\text{NIS})}, \quad (2)$$

- *F*: the free concentration of T<sub>4</sub> (ppm) in the supernatant.
- *B*: the amount of T<sub>4</sub> bound (adsorbed) by the polymer (mg of T<sub>4</sub> g<sup>-1</sup> of polyaniline) calculated by difference between the initial concentration of T<sub>4</sub> (ppm) and *F*.

As shown in Fig. 6, the reduction in concentration of thyroxine in case of MIP could be due to rebinding in the cavities. The reduction in the concentration of thyroxine in case of NIP could be attributed to the entrapment of thyroxine in the polymeric layers during centrifugation.

The higher the value of imprinting factor, the higher is the specific interactions with the polymer. The imprinting factor was found to be 1.98. It indicates that T<sub>4</sub> binds to the cavities formed in the polymer matrix. These data are complimented by the incubation study discussed under Sect. 3.3 [30].

### 3.2 Characterization of polyaniline and imprinting polyaniline matrix

Characterization studies for MIP, NIP, polyaniline with thyroxine, and pure thyroxine were performed using FT-IR (Fig. 7A and B). Figure 7A shows the characteristic peaks of polyaniline. Peak at 3460 cm<sup>-1</sup> denotes N–H stretching, 1630 cm<sup>-1</sup> denotes C=C stretching, and 1180 cm<sup>-1</sup> denotes—stretching [31]. In Fig. 7B, the 1100–400 cm<sup>-1</sup> scale has been zoomed to highlight the comparison between imprinted and non-imprinted polyaniline. Thyroxine structure has four carbon-iodine bonds (C–I bonds) which show a characteristic absorption between 670 and 680 cm<sup>-1</sup>. NIP has no thyroxine molecules; hence, there is a dip observed near 670 cm<sup>-1</sup>.

In MIP+T<sub>4</sub>, the presence of thyroxine is evident from the disappearance of the dip near 670 cm<sup>-1</sup> due to strong stretching vibrational frequency of C–I bond. On extracting thyroxine molecule from polyaniline matrix, the FT-IR spectra show a dip again.

The FT-IR results confirm the presence of thyroxine in polyaniline matrix in MIP+T<sub>4</sub> and absence of thyroxine in MIP generated after sonication. The previously shown HPLC data for the removal of T<sub>4</sub> compliment FT-IR data as the supernatant shows T<sub>4</sub> in the form of single peak at 10 min.

Contact angle studies were performed to study changes in surface energy or thyroxine imprinted polyaniline and comparing it with non-imprinted polyaniline coated on glass surface. The contact angle for NIP with water and ethylene glycol was found to be 54.2° and 27.3° as compared to 80.7° and 63.2° for MIP (as shown in Fig. 8a and b).

**Table 3** Trials with different parameters for studying thyroxine removal from polyaniline

Run	Conc. of NaOH (mM)	Temperature (°C)	Time (min)	Peak area in HPLC (a.u.)
1	125	30	30	2694652
2	100	30	45	2606173
3	75	40	45	2389787
4	100	30	15	1910671
5	75	30	30	2792259
6	100	40	30	2240712
7	100	50	15	2994670
8	100	40	30	2240712
9	125	40	15	1404862
10	75	50	30	2043485
11	100	50	45	1628344
12	125	50	30	1371182
13	75	40	15	4881631
14	125	40	45	1279771

**Fig. 5** Contour plot to study effect of temperature and molarity on removal of T<sub>4</sub> from polyaniline matrix

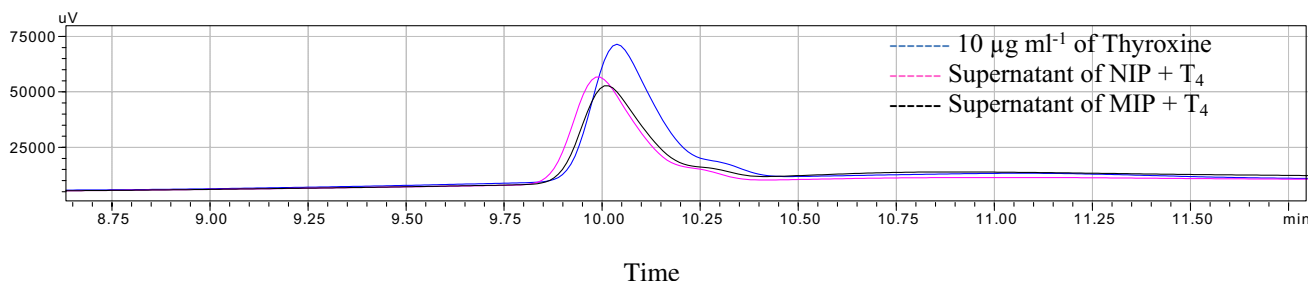
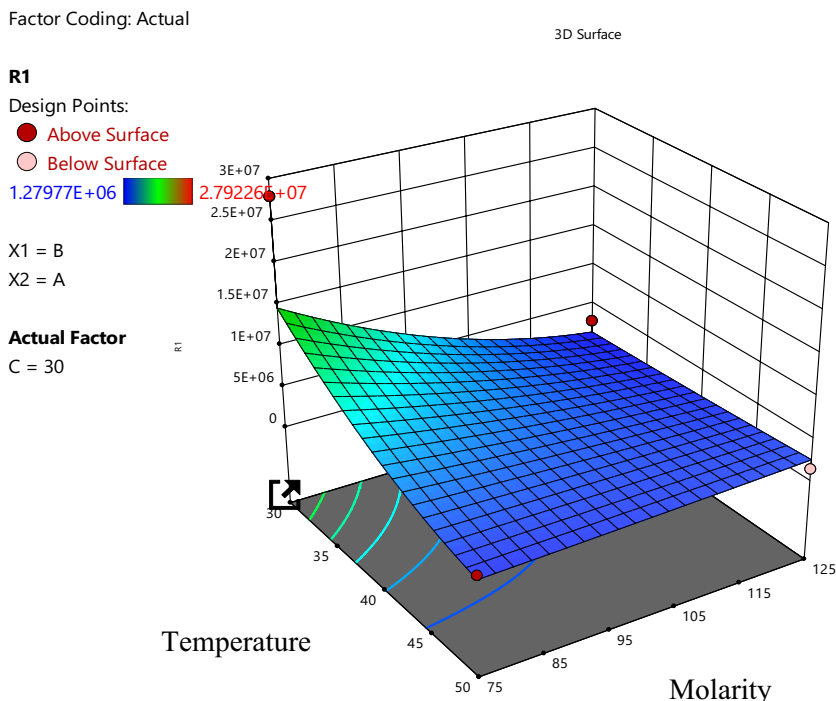


**Fig. 6** HPLC chromatogram shows peaks for 10 µg mL<sup>-1</sup> solution of T<sub>4</sub>, supernatant collected after mixing NIP with 10 µg mL<sup>-1</sup> solution of T<sub>4</sub> for 3 h and supernatant collected after mixing MIP with 10 µg

mL<sup>-1</sup> solution of T<sub>4</sub> for 3 h. These cavities in polyaniline matrix were then further characterized using FT-IR, AFM and contact angle studies

This shows that the removal of thyroxine forms cavities in the polyaniline matrix resulting in the roughness of polyaniline surface. The surface energy of MIP and NIP films was calculated using Fowkes equation (Eq. 3) [32].

$$1 + \cos \theta = 2\sqrt{\gamma_s^d \left( \frac{\sqrt{\gamma_1^d}}{\gamma_1} \right)} + 2\sqrt{\gamma_s^p \left( \frac{\sqrt{\gamma_1^p}}{\gamma_1} \right)} \quad (3)$$

where  $\theta$  = contact angle at solid–liquid interface;  $\gamma_s^d$  = dispersive component of solid surface energy;  $\gamma_s^p$  = polar component of solid surface energy;  $\gamma_1^d$  = dispersive component of liquid surface energy;  $\gamma_1^p$  = polar component of liquid surface energy;  $\gamma_1$  = total liquid surface energy.

The values of polar and dispersive components for water are reported to be 51.00 mJ m<sup>-2</sup> and 21.80 mJ m<sup>-2</sup> and for ethylene glycol, these values are 18.91 and 29.29 mJ m<sup>-2</sup>, respectively. Total liquid surface energy for water and ethylene glycol is calculated to be 72.80 and 48.20 mJ m<sup>-2</sup>, respectively. Putting these values in Eq. (3), the solid surface energies of MIP and NIP were calculated (Table 4). The total surface ( $\gamma_s$ ) of NIP was found to be higher than that of MIP. Due to formation of thyroxine cavities in the MIP, the contact angle was higher than NIP and the surface energy was subsequently lower [32].

Atomic force microscope analysis was done to find the surface topology and three-dimensional surface profile. Fig. 9 shows significant change in the morphology. The



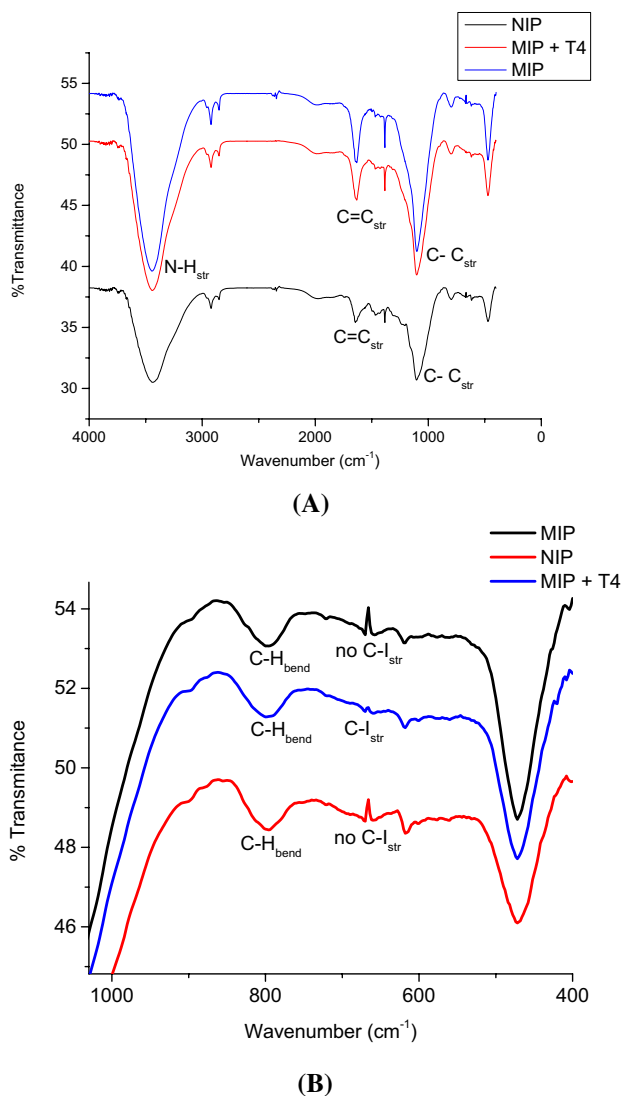


**Fig. 7** **A** Shows the scan range of 4000–400 cm<sup>-1</sup> MIP, NIP and thyroxine rebound MIP (MIP+T<sub>4</sub>) and **B** shows zoomed FT-IR scan of range 1100–400 cm<sup>-1</sup> for MIP, NIP, and thyroxine rebound MIP (MIP+T<sub>4</sub>)

surface roughness was calculated using WSxM software and it was found to be 1.02 nm for NIP and 5.04 nm for MIP [33]. The roughness can be due to small-scale variations in the height of a surface. Further, it can be attributed to the fact that due to the removal of thyroxine from MIP, the cavities were formed which resulted in increased surface roughness. The results were found to compliment the observations obtained in contact angle analysis, as the latter was found to be higher in MIP which is attributed to increased surface roughness [34].

The results obtained by HPLC, FT-IR, contact angle, and AFM prove that thyroxine was removed from the polyaniline matrix by sonication and resulting in the formation of MIPs.

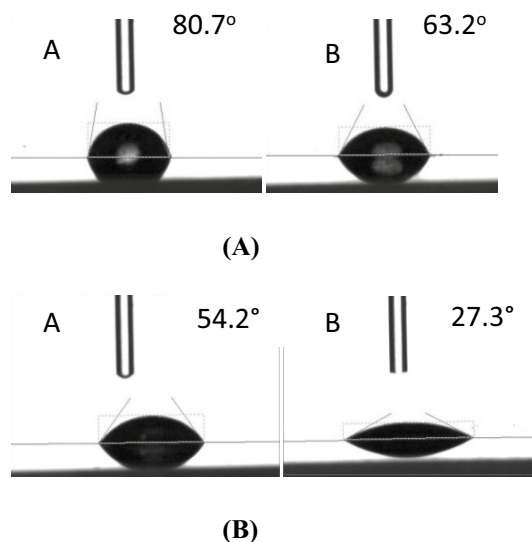


**Fig. 8** **a** Contact angle for MIP with water (A) and ethylene glycol (B). **b** Contact angle for NIP with water (A) and ethylene glycol (B)

### 3.3 Electrochemical analysis

#### 3.3.1 Electrochemical characterization

The response at various stages of MIP sensor fabrication was initially studied using CV and EIS (Fig. 10A and B).

The pristine ITO surface exhibits a peak anodic current ( $I_{pa}$ ) ~ 200  $\mu$ A. However, its modification with the imprinted PANI film results in an increase in  $I_{pa}$  ~ 350  $\mu$ A which is higher than that observed in pristine ITO and can be attributed to the presence of a conducting thin polymeric film [35]. The  $I_{pa}$  for MIP is slightly less than NIP which shows that there is very small change in conductance due to formation of cavities. However, on addition of thyroxine (50  $\mu$ g mL<sup>-1</sup>) on imprinted PANI,  $I_{pa}$  significantly decreases to ~ 210  $\mu$ A. But the addition of thyroxine to NIP does not show any change (discussed in incubation study in subsequent section).

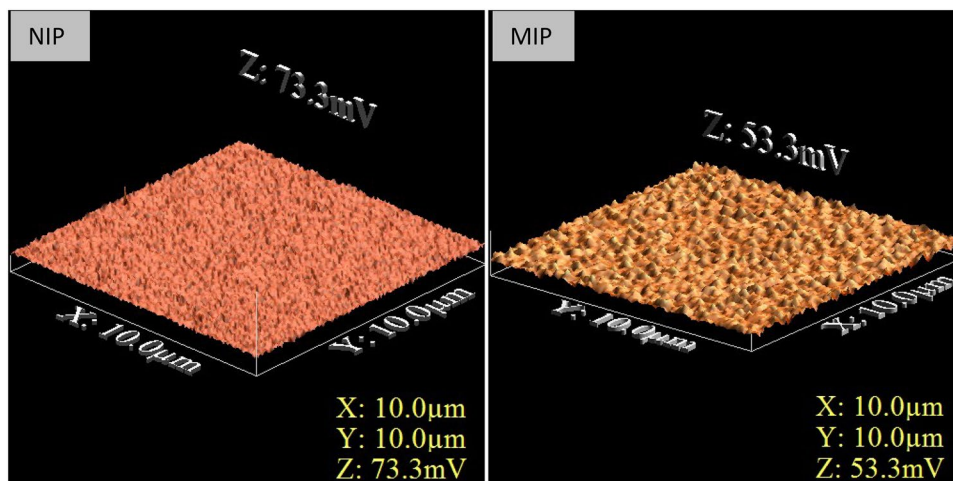
The EIS spectra in Fig. 10b complement the voltammograms of Fig. 10a, with high charge transfer resistance ( $R_{ct}$ ) in T<sub>4</sub>-bound PANI which comparatively decreases after the removal process. Insights onto interface kinetics at various sensor fabrication stages were studied using circuit simulation of Randel's equivalent model, and the latter is shown in Fig. 10b inset. The movement of bulk components on the electrode interface with frequency varying signal gives enhanced insights into the charge transfer process. Table 5 shows the simulated values for circuit elements.

The NIP surface exhibits a low charge transfer resistance ( $R_{ct}$ ) ~ 50 k $\Omega$ , as compared to MIP, which essentially is due to the high conductivity of polyaniline layer. The charge transfer becomes slightly more hindered in MIP as

**Table 4** Polar, dispersive, and total solid surface energy of NIP and MIP calculated using water and ethylene glycol contact angles

S. No	Solid surface	Contact angle (water)	Contact angle (ethylene glycol)	$\gamma_s^p$ (mJ m <sup>-2</sup> )	$\gamma_s^d$ (mJ m <sup>-2</sup> )	$\gamma_s$ (mJ m <sup>-2</sup> )
1	NIP	54.2°	27.3°	62.2	- 1.01	61.1
2	MIP	80.7°	63.2°	34.8	- 0.64	34.16

**Fig. 9** AFM images of MIP and NIP at 10 × 10 μm resolution



compared to NIP due to the formation of cavities. MIP has an ( $R_{ct}$ ) ~ 57 kΩ. Thyroxine rebound to polyaniline exhibits significant  $R_{ct}$  ~ 78k Ω. Such high  $R_s$  is attributed to the hindrance offered by embedded thyroxine in polyaniline matrix to the interfacial electron transfer.

When thyroxine re-binds to cavities in MIP, it serves to impede the electron transfer at electrode–electrolyte interface which results in low current or high impedance. Hence, it must be noted that thyroxine neither contribute to ionic current and hence nor toward electrode conductivity of the working electrode [32].

Therefore, the distinct response at each stage of sensor fabrication observed in CV and EIS indicates successful fabrication of molecularly imprinted polyaniline-based sensor for the selective recognition of  $T_4$ .

Furthermore, the electroactive surface area of  $T_4$  templated PANI electrodes was found by studying the current response at different scan rates (Fig. 11a).

The peak anodic and cathodic currents increase as the scan rate is elevated from 10 to 180 mV s<sup>-1</sup>, with the response saturating at the latter value. It can also be observed from Fig. 11a that the voltametric profile of the ferrocyanide redox probe is preserved at higher scan rates, thereby indicating the electrochemical stability within a vast scan rate range. Figure 11b and c establishes a direct proportionality of peak anodic current ( $I_{pa}$ ) and peak cathodic current ( $I_{pc}$ ) with square root of scan rate ( $\nu$ ), which corresponds to the well-known Randel’s–Sevick

(R–S) behavior. The electroactive surface area was therefore found to be 0.0011 cm<sup>2</sup> using the Eq. (4) [36].

Between the scan rate 50 and 180 mV s<sup>-1</sup>, the electrode process was found to be diffusion controlled as the anodic peak current ( $I_{pa}$ ) increased linearly with square root of scan rate [34].

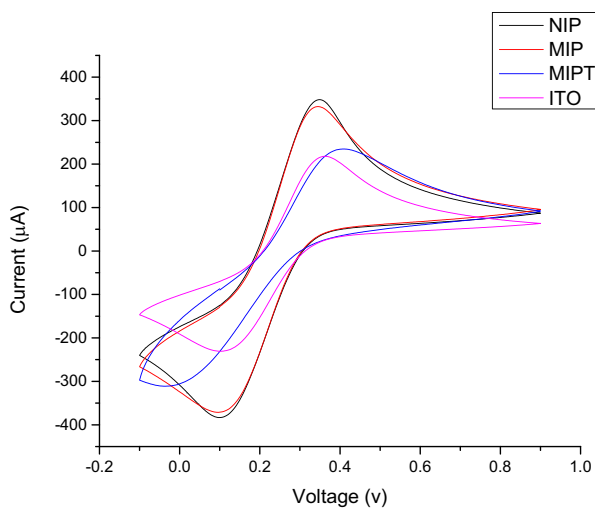
$$I_{pa}(\mu A) = 19.02 + 0.039\nu^{1/2}(\text{V s}^{-1}) \quad r^2 = 0.986. \quad (4)$$

Incubation study was performed to understand the optimal contact time of thyroxine with the MIP-coated ITO. The following Table 6 shows the response reduction with increase in incubation time. After 8 min, the response becomes constant. A slightly higher time, i.e., 10 min, was selected as the optimal time. NIP was also incubated with 50 pg mL<sup>-1</sup> of thyroxine and no change in response was observed for NIP (as shown in Fig. 12). This observation shows the absence of any significant non-specific binding of thyroxine on the polymer matrix.

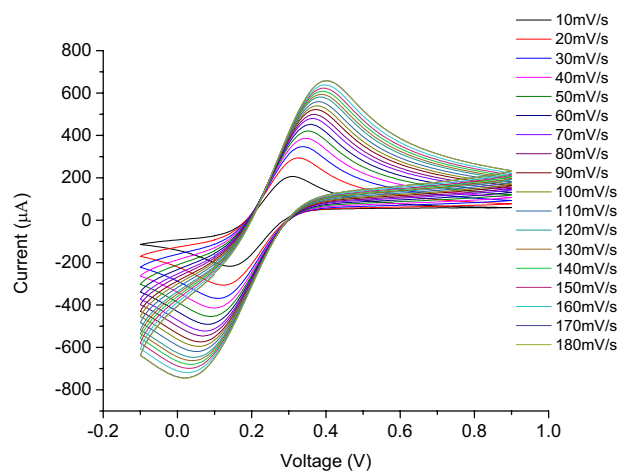
### 3.3.2 Analytical sensor performance

The analytical response of the developed MIP sensor at various  $T_4$  concentrations was studied using CV, as shown in Fig. 13a.

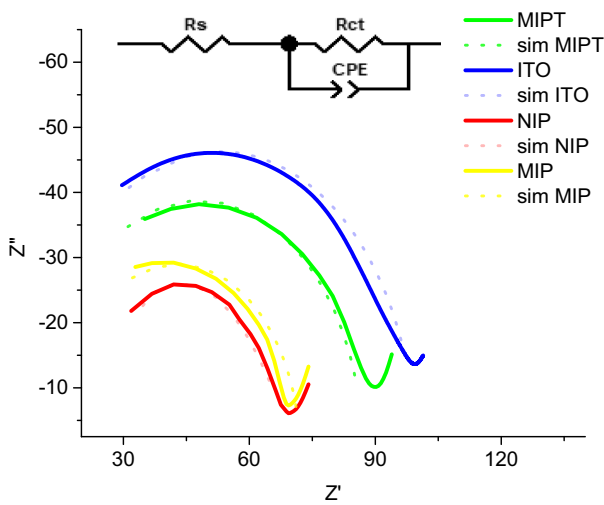
It can be observed that the  $I_{p,a}$  decreases from 500 μA to 400 μA as  $T_4$  concentration is elevated from 5 pg mL<sup>-1</sup> to 50 pg mL<sup>-1</sup>. This can be attributed to the formation of partial



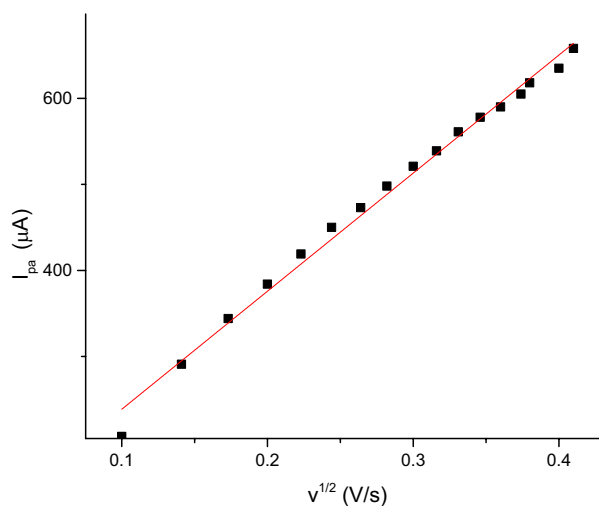
(A)



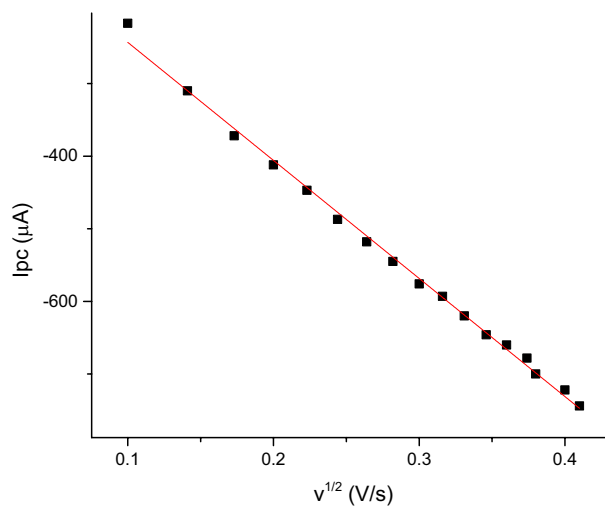
(A)



(B)



(B)



(C)

**Fig. 10** **A** Current and voltage profile for NIP, MIP,  $T_4$  rebound to MIP and ITO. **B** Nyquist plot for bare ITO, NIP, MIP, and  $T_4$  rebound MIP. The dotted lines show the simulated plots obtained using Zview software. Randle’s circuit stimulates the impedance data

**Table 5** Simulated values of circuit elements incorporated for modeling the sensor electrolyte interface, for MIP and NIP

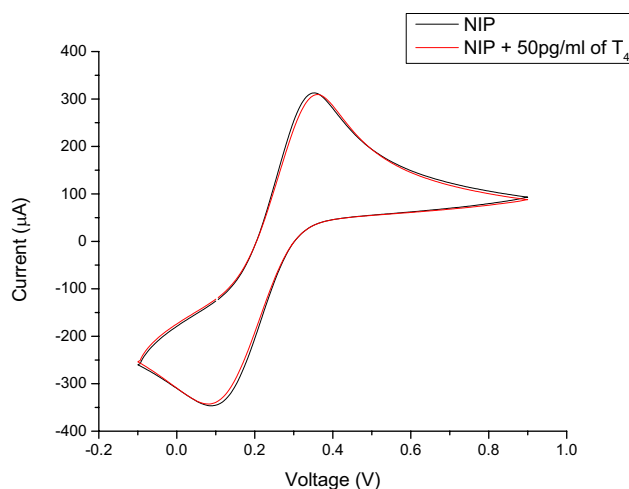
Surface	Series resistance $R_s$ (k $\Omega$ )	Charge transfer resistance $R_{ct}$ (k $\Omega$ )	Constant phase element CPE (F)
NIP	19	50	$3.9 \times 10^{-8}$
MIP	13	57	$6 \times 10^{-8}$

surface passivation, at higher  $T_4$  concentrations, resulting in significant impediments to the interfacial electron transfer. The developed sensor was calibrated at 0.36 V, resulting in a linear relation between  $I_{p.a.}$  and  $T_4$  concentration, shown

**Fig. 11** **a** Study of scan rate vs current response from 10 to 180  $\text{mV s}^{-1}$ . **b** Change of peak anodic current ( $I_{pa}$ ) with  $v^{1/2}$ . **c** Change of peak anodic current ( $I_{pc}$ ) with  $v^{1/2}$

**Table 6** Change in anodic current with respect to time

Time (min)	Reduction of peak current (%) in NIP	Reduction of current (%) in MIP
2	1.1	1.6
4	1.2	4.2
6	1.1	6.4
8	1.6	37
10	1.2	41
12	1.2	42
14	1.2	42

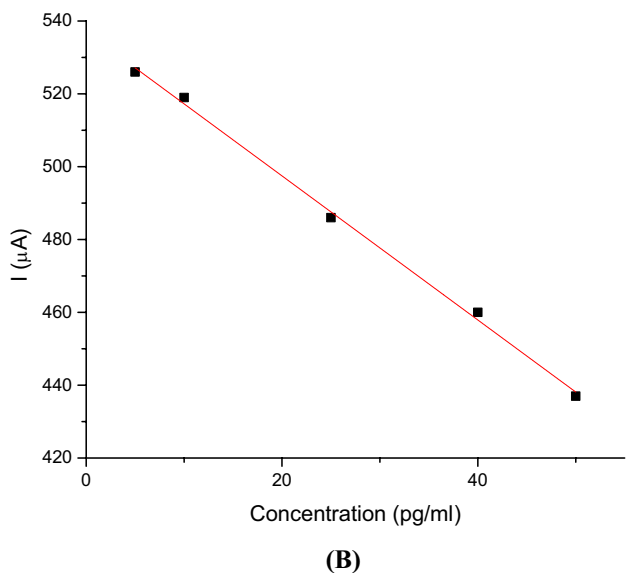
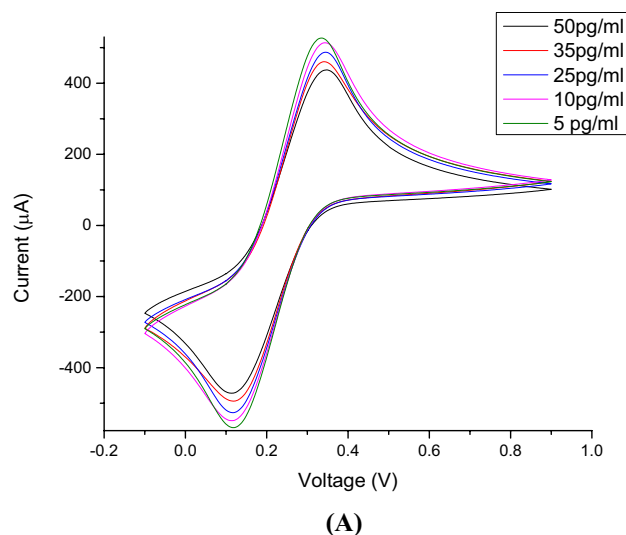
**Fig. 12** CV curve for NIP and NIP incubated with 50 pg mL<sup>-1</sup> of T<sub>4</sub>

in Fig. 13b. The variation in response at this potential was found linear with change in concentration. The linear equation is  $y = -1.978x + 537.03$  and  $r^2 = 0.9978$ .

The limit of detection (LoD) was calculated using the 3 $\sigma$  rule and was found to be 6.16 pg mL<sup>-1</sup> [18]. In the repeatability test, the response of 5 independently fabricated electrodes were measured for thyroxine (50 pg mL<sup>-1</sup>). The relative standard deviation was calculated as 2.45%.

The sensor parameters of developed MIP-based platform were compared with few previously reported studies, as highlighted in Table 7. The method was found to be more sensitive than other techniques. The method covers the normal range of free thyroxine present in the blood as well as saliva.

The developed T<sub>4</sub> imprinted polyaniline sensor electrodes were further subjected to various potential interferants, and the corresponding response was obtained using CV technique. The CV response of T<sub>4</sub> along with chosen interferants such as phenylalanine (Phe), tyrosine (Tyr), and liothyronine (Lio) was observed for the interference studies. As shown in Fig. 14, the percentage relative binding for other compounds

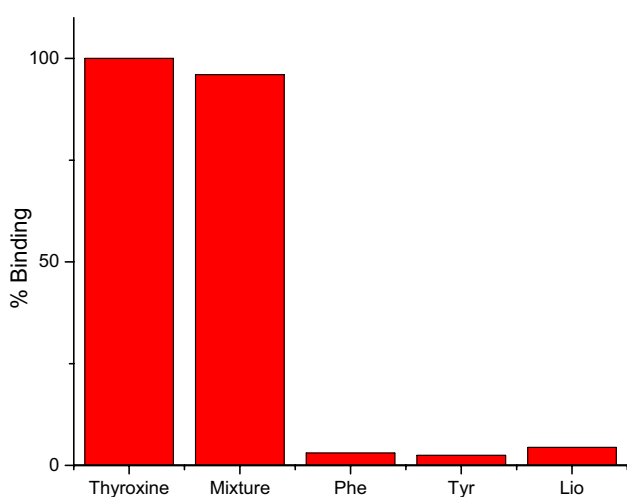
**Fig. 13** a CV profile for different concentration of thyroxine solutions. b Linearity curve for 5–50 pg mL<sup>-1</sup> concentration range

was phenylalanine (1.3%), tyrosine (1.7%), and liothyronine (3.1%). The mixture denotes presence of all interfering compounds and thyroxine.

It can be observed that the interferants has insignificant binding capabilities in the templated PANI matrix as indicated by the % binding values mentioned above, which justifies the presence of T<sub>4</sub>-specific cavities. To conduct a real sample analysis, molecularly imprinted PANI sensor was used for the determination of T<sub>4</sub> (50 pg mL<sup>-1</sup>) in human saliva. The average recovery observed was 107% (range 96–115.2%) and relative standard deviation was 0.98%. The upper limit of recovery was observed to be slightly on the higher side because of the presence of natural thyroxine in saliva. The levels of free thyroxine in saliva are also in pg mL<sup>-1</sup> levels and are comparable to the blood levels. Hence,

**Table 7** Comparison of sensitivity other techniques for determination of thyroxine

Electrode	Materials used	Method	LOD (nM)	References
Screen printed electrode	Carbon nanotubes, graphene, and gold nanoparticles	Differential pulse voltammetry	30	[37]
Renewable mercury film silver-based electrode	Renewable mercury film	Cyclic voltammetry	18	[38]
Carbon paste electrode	Graphite powder in paraffin oil	Cyclic voltammetry	6.5	[39]
Gold microgap electrode	Thyroxine DNA aptamer/rhodium nanoplate heterolayer	Cyclic voltammetry and electrochemical impedance spectroscopy	0.01	[5]
Modified copper disk and PVC tube	Reduced graphene oxide containing gold nanoparticles attached with beta-cyclodextrin	Amperometry	1	[39]
Indium tin oxide-coated glass	Molecularly imprinted polyaniline	Cyclic voltammetry	0.0079	Present study

**Fig. 14** Effect of potential interfering compounds on the response of molecularly imprinted PANI sensor toward the detection of T<sub>4</sub>

this method can be used for the determination of thyroxine in saliva [40].

The promising analytical sensor performance therefore highlights the potential of the developed platform to be translated toward clinical applications in a point-of-care scenario, for increased patient outcomes [34].

## 4 Conclusion

Molecularly imprinted polyaniline was synthesized and applied for the determination of thyroxine using cyclic voltammetry. Optimization studies were done for the removal of thyroxine from polyaniline matrix which is a critical step for the synthesis of MIP. The characterization studies using AFM, contact angle, and FT-IR confirmed that the imprinting was successful. The results from these techniques complemented those obtained through chromatographic analysis

using HPLC. The imprinted polymer was coated onto ITO surface used as a working electrode for electrochemical analysis. Linearity was obtained for a range of 5–50 pg mL<sup>-1</sup> and limit of detection was found to be 6.16 pg mL<sup>-1</sup>. The method was found to be more sensitive than other reported techniques. It shows good recovery in saliva which is a useful non-invasive biological matrix for the diagnosis of diseases. However, the reference range in saliva is still to be harmonized. This method can be used for the estimation of salivary thyroxine in human population and correlating it with the status of thyroid disease. The result of the study is a step forward toward the development of a robust MIP-based biosensor that can be used for developing a highly selective point-of-care device for thyroxine in biological matrices.

**Acknowledgements** The authors would sincerely like to thank University of Petroleum and Energy Studies for providing SEED funds (HS/23032020/01) to perform the studies, Mcleods Pharmaceutical Limited for providing the active pharmaceutical compound (thyroxine). Daljit Kaur, Dr. Tejdeep Kaur and Parvinder Singh for their support during the study. Authors are also thankful to Dr. Tapas Goswami for helping in the synthesis of polyaniline and characterization studies.

**Author contributions** DS did the practical experiments. SR assisted in planning the experiments and data analysis. NM helped in data analysis, correction, and revision of the manuscript. AM helped in planning, data analysis, manuscript writing, evaluation of the results, and reviewing and correction of the manuscript. All authors reviewed the manuscript.

## Declarations

**Competing interest** The authors declare no competing interests.

## References

1. Taylor P, Albrecht D, Scholz A et al (2018) Global epidemiology of hyperthyroidism and hypothyroidism. *Nat Rev Endocrinol*. <https://doi.org/10.1038/nrendo.2018.18>



2. Couto RAS, Gonçalves LM, Góes MS et al (2017) SAM-based immunosensor for the analysis of thyroxine ( $T_4$ ). *J Electrochem Soc* 164:B103. <https://doi.org/10.1149/2.0561704jes>
3. Sharma S, Byrne H, O'Kennedy RJ (2016) Antibodies and antibody-derived analytical biosensors. *Essays biochem* 60:9–18. <https://doi.org/10.1042/ebc20150002>
4. Pantalone KM, Hatipoglu B, Gupta MK et al (2015) Measurement of serum free thyroxine Index may provide additional case detection compared to free thyroxine in the diagnosis of central hypothyroidism. *Case Rep Endocrinol* 2015:965191. <https://doi.org/10.1155/2015/965191>
5. Park SY, Kim J, Yim G et al (2020) Fabrication of electrochemical biosensor composed of multi-functional DNA/rhodium nanoplate heterolayer for thyroxine detection in clinical sample. *Colloids Surf B Biointerfaces* 195:111240. <https://doi.org/10.1016/j.colsurfb.2020.111240>
6. Romero-Gómez B, Guerrero-Alonso P, Carmona-Torres JM et al (2019) Mood disorders in levothyroxine-treated hypothyroid women. *Int J Environ Res Public Health* 16:4776. <https://doi.org/10.3390/ijerph16234776>
7. McConnell EM, Nguyen J, Li Y (2020) Aptamer-based biosensors for environmental monitoring. *Front Chem* 8:434. <https://doi.org/10.3389/fchem.2020.00434>
8. Rocchitta G, Spanu A, Babudieri S et al (2016) Enzyme biosensors for biomedical applications: strategies for safeguarding analytical performances in biological fluids. *Sensors* 16:780. <https://doi.org/10.3390/s16060780>
9. Fopase R, Paramasivam S, Kale P et al (2020) Strategies, challenges and opportunities of enzyme immobilization on porous silicon for biosensing applications. *J Environ Chem Eng* 8:104266. <https://doi.org/10.1016/j.jece.2020.104266>
10. Giuliano K, Grant M (2002) Blood analysis at the point of care: issues in application for use in critically ill patients. *AACN Clin Issues* 13:204–220. <https://doi.org/10.1097/00044067-200205000-00006>
11. Menger M, Yarman A, Erdőssy J et al (2016) MIPs and aptamers for recognition of proteins in biomimetic sensing. *Biosensors* 6:35. <https://doi.org/10.3390/bios6030035>
12. Vasapollo G, Sole RD, Mergola L et al (2011) Molecularly imprinted polymers: present and future prospective. *Int J Mol Sci* 12:5908–5945. <https://doi.org/10.3390/ijms12095908>
13. Ermiş N, Tinkiliç N (2021) Development of an electrochemical sensor for selective determination of dopamine based on molecularly imprinted poly(p-aminothiophenol) polymeric film. *Electroanalysis* 33:1491–1501. <https://doi.org/10.1002/elan.202060556>
14. Ermiş N, Uzun L, Denizli A (2017) Preparation of molecularly imprinted electrochemical sensor for L-phenylalanine detection and its application. *J Electroanal Chem* 807:244–252. <https://doi.org/10.1016/j.jelechem.2017.11.025>
15. Chuiprasert J, Srinives S, Boontanon N et al (2023) Electrochemical sensor based on a composite of reduced graphene oxide and molecularly imprinted copolymer of polyaniline–poly(o-phenylenediamine) for ciprofloxacin determination: fabrication, characterization, and performance evaluation. *ACS Omega* 8:2564–2574. <https://doi.org/10.1021/acsomega.2c07095>
16. Ndunda EN, Mizaikoff B (2016) Molecularly imprinted polymers for the analysis and removal of polychlorinated aromatic compounds in the environment: a review. *Analyst* 141:3141–3156. <https://doi.org/10.1039/C6AN00293E>
17. Nagabooshanam S, Roy S, Deshmukh S et al (2020) Microfluidic affinity sensor based on a molecularly imprinted polymer for ultra-sensitive detection of chlorpyrifos. *ACS Omega* 5:31765–31773. <https://doi.org/10.1021/acsomega.0c04436>
18. Roy S, Nagabooshanam S, Wadhwa S et al (2020) Ultra-sensitive detection of L-tyrosine using molecularly imprinted electrochemical sensor towards diabetic foot ulcer detection. *Electrochem Comm* 117:106782. <https://doi.org/10.1016/j.elecom.2020.106782>
19. Rajpal S, Mishra P (2022) Next generation biosensors employing molecularly imprinted polymers as sensing elements for in vitro diagnostics. *Biosens Bioelectron X* 11:100201. <https://doi.org/10.1016/j.biosx.2022.100201>
20. Anirudhan TS, Mani A, Athira VS (2021) Molecularly imprinted electrochemical sensing platform for 2-amino adipic acid, a diabetes biomarker. *React Func Polym* 168:105056. <https://doi.org/10.1016/j.reactfunctpolym.2021.105056>
21. Yadav AK, Verma D, Dalal N et al (2022) Molecularly imprinted polymer-based nanodiagnosics for clinically pertinent bacteria and virus detection for future pandemics. *Biosens Bioelectron X* 12:100257. <https://doi.org/10.1016/j.biosx.2022.100257>
22. Regan B, Boyle F, O'Kennedy R et al (2019) Evaluation of molecularly imprinted polymers for point-of-care testing for cardiovascular disease. *Sensors* 19:3485. <https://doi.org/10.3390/s19163485>
23. Bhakta S, Mishra P (2021) Molecularly imprinted polymer-based sensors for cancer biomarker detection. *Sens Actuators* 3:100061. <https://doi.org/10.1016/j.snr.2021.100061>
24. Maout PL, Wojkiewicz J-L, Redon N et al (2018) Polyaniline nanocomposites based sensor array for breath ammonia analysis. portable e-nose approach to non-invasive diagnosis of chronic kidney disease. *Sens Actuators B Chem* 274:616–626. <https://doi.org/10.1016/j.snb.2018.07.178>
25. Abu-Thabit NY (2016) Chemical oxidative polymerization of polyaniline: a practical approach for preparation of smart conductive textiles. *J Chem Educ* 93:1606–1611. <https://doi.org/10.1021/acs.jchemed.6b00060>
26. Collier JW, Shah RB, Bryant AR et al (2011) Development and application of a validated HPLC method for the analysis of dissolution samples of levothyroxine sodium drug products. *J Pharm Biomed Anal* 54:433–438. <https://doi.org/10.1016/j.jpba.2010.08.025>
27. Neu V, Bielow C, Schneider P et al (2013) Investigation of reaction mechanisms of drug degradation in the solid state: a kinetic study implementing ultrahigh-performance liquid chromatography and high-resolution mass spectrometry for thermally stressed thyroxine. *Anal Chem* 85:2385. <https://doi.org/10.1021/ac303404e>
28. Hudson AD, Solà R, Ueta JT et al (2019) Synthesis of optimized molecularly imprinted polymers for the isolation and detection of antidepressants via HPLC. *Biomimetics* 4:18
29. Singh D, Bansal A, Jain A et al (2021) GC-MS based lemon grass metabolite analysis involved in the synthesis of silver nanoparticles and evaluation of photo-catalytic degradation of methylene blue. *Biometals* 34:1121–1139. <https://doi.org/10.1007/s10534-021-00337-6>
30. Lafarge C, Bitar M, Hosry LE et al (2020) Comparison of molecularly imprinted polymers (MIP) and sol–gel molecularly imprinted silica (MIS) for fungicide in a hydro alcoholic solution. *Mater Today Commun* 24:101157. <https://doi.org/10.1016/j.mtcomm.2020.101157>
31. Shao W, Jamal R, Xu F et al (2012) The effect of a small amount of water on the structure and electrochemical properties of solid-state synthesized polyaniline. *Materials* 5:1811–1825. <https://doi.org/10.3390/ma5101811>
32. Roy S, Nagabooshanam S, Chauhan N et al (2021) Design and development of a novel flexible molecularly imprinted electroanalytical sensor for the monitoring of diabetic foot ulcers. *Surf Interfaces* 26:101310. <https://doi.org/10.1016/j.surfint.2021.101310>
33. Hu C, He Q, Li Q et al (2004) Enhanced reduction and determination of trace thyroxine at carbon paste electrode in the presence of



- trace cetyltrimethylammonium bromide. *Anal Sci* 20:1049–1054. <https://doi.org/10.2116/analsci.20.1049>
34. Prasad BB, Madhuri R, Tiwari MP et al (2010) Layer-by-layer assembled molecularly imprinted polymer modified silver electrode for enantioselective detection of D- and L-thyroxine. *Anal Chim Acta* 681:16–26. <https://doi.org/10.1016/j.aca.2010.09.027>
35. Crapnell RD, Dempsey-Hibbert NC, Peeters M et al (2020) Molecularly imprinted polymer based electrochemical biosensors: overcoming the challenges of detecting vital biomarkers and speeding up diagnosis. *Talanta Open* 2:100018. <https://doi.org/10.1016/j.talo.2020.100018>
36. Zhu P, Zhao Y (2019) Cyclic voltammetry measurements of electroactive surface area of porous nickel: peak current and peak charge methods and diffusion layer effect. *Mater Chem Phys* 233:60–67. <https://doi.org/10.1016/j.matchemphys.2019.05.034>
37. David M, Șerban A, Enache TA et al (2022) Electrochemical quantification of levothyroxine at disposable screen-printed electrodes. *J Electroanal Chem* 911:116240. <https://doi.org/10.1016/j.jelechem.2022.116240>
38. Smajdor J, Piech R, Rumin M et al (2016) High sensitive voltammetric levothyroxine sodium determination on renewable mercury film silver based electrode. *J Electrochem Soc* 163(9):H605–H609. <https://doi.org/10.1149/2.1431607jes>
39. Muñoz J, Riba-Moliner M, Brennan LJ et al (2016) Amperometric thyroxine sensor using a nanocomposite based on graphene modified with gold nanoparticles carrying a thiolated  $\beta$ -cyclodextrin. *Microchim Acta* 183:1579–1589. <https://doi.org/10.1007/s00604-016-1783-x>
40. Higashi T, Ichikawa T, Shimizu C et al (2011) Stable isotope-dilution liquid chromatography/tandem mass spectrometry method for determination of thyroxine in saliva. *J Chromatogr B* 879:1013–1017. <https://doi.org/10.1016/j.jchromb.2011.02.048>

**Publisher's Note** Springer Nature remains neutral with regard to jurisdictional claims in published maps and institutional affiliations.

Springer Nature or its licensor (e.g. a society or other partner) holds exclusive rights to this article under a publishing agreement with the author(s) or other rightsholder(s); author self-archiving of the accepted manuscript version of this article is solely governed by the terms of such publishing agreement and applicable law.